


**Topological defects, inherent structures, and hyperuniformity**Duyu Chen<sup>1,\*</sup>, Yu Zheng<sup>2</sup>, and Yang Jiao<sup>3,2,†</sup><sup>1</sup>*Materials Research Laboratory, University of California, Santa Barbara, California 93106, USA*<sup>2</sup>*Department of Physics, Arizona State University, Tempe, Arizona 85287, USA*<sup>3</sup>*Materials Science and Engineering, Arizona State University, Tempe, Arizona 85287, USA* (Received 18 July 2021; revised 21 October 2021; accepted 25 October 2021; published 1 November 2021)

A wide spectrum of disordered many-body systems that are inherent structures (i.e., local minima of potential energy landscape) was recently discovered to possess a novel hidden long-range order known as hyperuniformity, yet the mechanisms associated with the emergence of disordered hyperuniformity in such systems are not well understood. Here, we address this important fundamental problem by linking together the concepts of topological defects, inherent structures, and hyperuniformity. We consider representative examples of disordered inherent structures that are topological variants of crystals obtained by continuously introducing into the crystalline state randomly distributed topological defects such as dislocations and disclinations. Using large-scale numerical simulations and analysis based on a continuum theory, we show that the topological defects and the associated transformation pathways linking the disordered inherent structures to the crystalline state preserve hyperuniformity of the latter, as long as the displacements induced by the defects are sufficiently localized (i.e., the volume integrals of the displacements and squared displacements caused by individual defect are finite) and the displacement-displacement correlation matrix of the system is diagonalized and isotropic. Our results provide insights to the discovery, design, and generation of novel disordered hyperuniform materials.

DOI: [10.1103/PhysRevB.104.174101](https://doi.org/10.1103/PhysRevB.104.174101)**I. INTRODUCTION**

Very recently, it was discovered that a wide spectrum of disordered many-body systems can possess a remarkable property called “hyperuniformity.” Disordered hyperuniform (DHU) systems are exotic states of matter [1,2] that lie between a perfect crystal and liquid. These systems are similar to liquids or glasses in that they are statistically isotropic and possess no Bragg peaks, and yet they completely suppress large-scale normalized density fluctuations like crystals and in this sense possess a hidden long-range order [1–3]. Specifically, the static structure factor  $S(k)$  vanishes for DHU systems in the infinite-wavelength (or zero-wave-number) limit, i.e.,  $\lim_{k \rightarrow 0} S(k) = 0$ , where  $k$  is the wave number [1,2]. Here,  $S(k)$  is defined as  $S(k) \equiv 1 + \rho \tilde{h}(k)$ , where  $\tilde{h}(k)$  is the Fourier transform of the total correlation function  $h(r) = g_2(r) - 1$ ,  $g_2(r)$  is the pair correlation function, and  $\rho$  is the number density of the system. Note that this definition implies that the forward scattering contribution to the diffraction pattern is omitted. Equivalently, the local number variance  $\sigma_N^2(R)$  associated with a spherical observation window of radius  $R$  grows more slowly than the window volume for DHU systems in the large- $R$  limit [1,2]. The small- $k$  scaling behavior of  $S(k) \sim k^\alpha$  dictates the large- $R$  asymptotic behavior of  $\sigma_N^2(R)$ , based on which all DHU systems can be categorized into three classes:  $\sigma_N^2(R) \sim R^{d-1}$  for  $\alpha > 1$  (class I),

$\sigma_N^2(R) \sim R^{d-1} \ln(R)$  for  $\alpha = 1$  (class II), and  $\sigma_N^2(R) \sim R^{d-\alpha}$  for  $0 < \alpha < 1$  (class III) [2].

DHU states have been discovered in a wide spectrum of equilibrium and nonequilibrium physical, biological, and chemical systems, and appear to endow such systems with novel physical properties [4–30]; see Ref. [2] for a thorough overview. While it is well known that effective long-range interactions are required to drive an equilibrium many-particle system to a hyperuniform state, this condition is not necessary to achieve hyperuniformity in systems out of equilibrium [2]. Among the wide spectrum of hyperuniform nonequilibrium systems discovered previously, many fall into the category of inherent structures, e.g., maximally random-jammed (MRJ) hard-particle packings [4–7,31], avian photoreceptor patterns [19], and the inherent structures associated with the  $k$ -space overlap potentials [32]. It is also noteworthy that certain inherent structures are found to be nonhyperuniform [32], e.g., the inherent structures associated with the Lennard-Jones and steeply repulsive potentials [32,33].

Despite the ubiquitous nature of disordered hyperuniform inherent structures, the mechanisms associated with the emergence of disordered hyperuniformity in many such systems are still not well understood. In this work, we link the concepts of topological defects and inherent structures to our fundamental understanding of the emergence of hyperuniformity. In particular, we consider a representative class of disordered inherent structures in two-dimensional Euclidean space  $\mathbb{R}^2$  which can be viewed as defected states of a perfect triangular lattice crystal [34,35] obtained by continuously introducing topological defects such as bound dislocations, free dislocations, and disclinations. Using large-scale numerical

\*duyu@alumni.princeton.edu

†yang.jiao.2@asu.edu

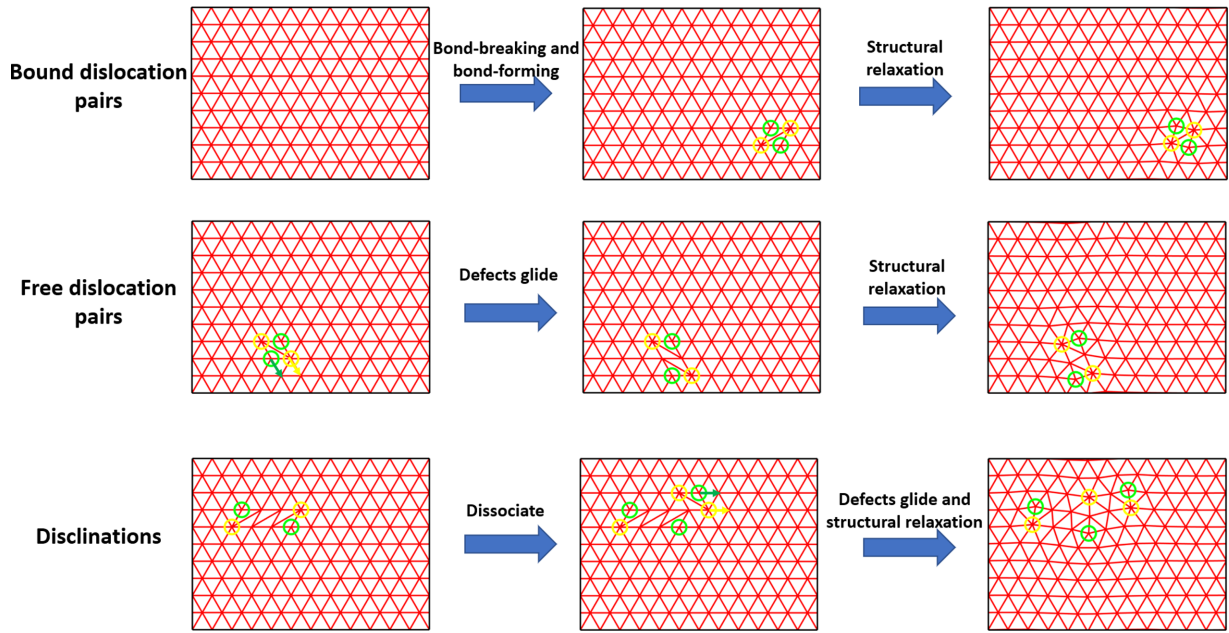


FIG. 1. Illustration of the formation of inherent structures containing bound dislocations (top panel), free dislocations (middle panel), and disclinations with associated dislocations (bottom panel) through a series of topological transformations (i.e., rearrangement of bonding network) and subsequent structural relaxation in a triangular lattice. Vertices with seven bonds are highlighted with yellow circles, and vertices with five bonds are highlighted with green circles.

simulations and continuum theory analysis, we demonstrate that the class-I hyperuniformity of the original crystal is preserved as long as the displacements induced by each individual defect decay sufficiently fast from the source (i.e., the volume integrals of the displacements and squared displacements caused by individual defect are finite) and the displacement-displacement correlation matrix of the system is diagonalized and isotropic.

The rest of the paper is organized as follows: in Sec II, we describe the procedures to generate disordered inherent structures via continuous topological transformations from the reference triangular lattice crystal state in  $\mathbb{R}^2$ . In Sec. III, we employ various statistical descriptors to characterize the large-scale structural features, in particular hyperuniformity of the resulting inherent structures. In Sec. IV, we derive continuum theory to explain the class-I hyperuniformity of the inherent structures. In Sec. V, we provide concluding remarks.

## II. REALIZATIONS OF DISORDERED INHERENT STRUCTURES CONTAINING RANDOMLY DISTRIBUTED TOPOLOGICAL DEFECTS

### A. Dislocations and disclinations induced by topological transformations

To introduce bound dislocations (i.e., a pair of dislocations that are next to each other) into the triangular lattice, we first randomly pick a bond in the lattice. Note that any bond in the triangular lattice is also the short diagonal of a rhombus. Next, we break this chosen bond and connect the two vertices associated with the long diagonal of the corresponding rhombus with a new bond, resulting in a pair of dislocations next to one another. If the vertices associated with the old and new bonds all possess six bonds before the transformation, then the trans-

formation would lead to two five-coordinated vertices and two seven-coordinated vertices; otherwise, we would obtain higher-order defected structures. Here we impose the constraint that the vertices after the transformation should each possess at least five bonds to ensure local structural stability. The process of introducing a single pair of bound dislocations is illustrated in the top panel of Fig. 1. We quantify the amount of bound dislocations by the defect concentration  $p$  in this context defined as  $p \equiv N_{op,1}/N_b$ , where  $N_{op,1}$  is the number of topological transformations described in this paragraph, and  $N_b$  is the number of bonds in the triangular lattice. Note that a single topological transformation described in this paragraph would introduce a pair of dislocations, in the absence of other topological defects.

To introduce free dislocations, we start from bound dislocations with the additional constraint that the initial bound dislocations should consist of two five-coordinated vertices and two seven-coordinated vertices, and randomly pick a five-coordinated vertex and a seven-coordinated vertex that are part of the bound dislocations. We then let these two defected vertices “glide” in the lattice by continuously breaking existing bonds and forming new bonds. Note that the direction that the defected vertices can glide is fixed once the two vertices are picked given the local bonding constraints. To form free dislocations and minimize the spatial correlations of the free dislocations, we let the defects glide for at least one step; beyond that, the defects have 1/2 of probability to stop and 1/2 of probability to continue gliding at each lattice site. If the gliding defects stop before hitting any “road block,” i.e., vertices that are not six coordinated, then we count this as one topological transformation in the context of free dislocations; otherwise, we restore the structure before this trial and start another attempt to insert a free dislocation. The process of

introducing a single pair of free dislocations is illustrated in the middle panel of Fig. 1. We also experiment with other stopping rules, and find that the details of different stopping rules do not affect the large-scale structural features of the resulting structures, which is the focus of this work. We quantify the amount of free dislocations by the defect concentration  $p$  in this context defined as  $p \equiv N_{op,2}/N_b$ , where  $N_{op,2}$  is the number of topological transformations described in this paragraph, and  $N_b$  is the number of bonds in the triangular lattice. Note that similar to the case of bound dislocations, a single topological transformation described in this paragraph would introduce a pair of dislocations (each consisting of a five-coordinated vertex and a seven-coordinated vertex), in the absence of other topological defects.

To introduce disclinations, we start from a free dislocation and break the bond between the seven-coordinated vertex and one of its six-coordinated neighbors and connect the long diagonal of the corresponding rhombus with a new bond. This six-coordinated neighbor should have two six-coordinated neighbors that are not a neighbor of the five-coordinated vertex. This bond-breaking and bond-forming process creates an isolated five-coordinated vertex, and another five-coordinated vertex surrounded by two seven-coordinated vertices. We then let one of the two seven-coordinated vertices and its neighboring five-coordinated vertex glide away in the same way as that in the case of free dislocations. If these steps can be completed, then we count this as a topological transformation in the context of disclinations, which would create an isolated fivefold disclination, an isolated sevenfold disclination, and two free dislocations (each consisting of a five-coordinated vertex and a seven-coordinated vertex), in the absence of other topological defects (such a topological transformation is illustrated in the bottom panel of Fig. 1). Otherwise, we restore the structure before this trial and start another attempt to insert a disclination. Note that the disclinations are accompanied by free dislocations, which is consistent with previous observations [36,37] that disclinations typically arise with free dislocations. We quantify the amount of disclinations by the defect concentration  $q$  defined as  $q \equiv N_{op,3}/N_b$ , where  $N_{op,3}$  is the number of topological transformations described in this paragraph, and  $N_b$  is the number of bonds in the triangular lattice. It is noteworthy that structures containing disclinations at  $q$  should be compared to structures containing bound and free dislocations at  $p = \frac{3}{2}q$  for a fair comparison at the same effective defect concentration, given the number of five-coordinated and seven-coordinated vertices that each case generates in the absence of other topological defects.

### B. Inherent structures

To obtain the inherent structures, we allow the transformed structures to undergo elastic relaxation by perturbing the positions of the vertices in a way that drives the bond lengths in the network towards values associated with the triangular lattice through Monte Carlo simulations. In particular, this involves local minimization of a harmonic energy  $E$  defined as follows:

$$E = \sum_{\text{bonds}} k_b (b_i - b_0)^2, \quad (1)$$

where  $b_i$  is the bond length associated with bond  $i$ , and  $b_0 = 1$  is the side length of a triangle in a triangular lattice. We note that the harmonic energy is a good approximation of particle interactions for many physical systems at low temperatures. Since we are looking at local energy minima, the choice of the spring constant  $k_b$  does not affect the obtained structure and, without loss of generality, we set  $k_b$  to unity. Specifically, in our Monte Carlo simulations, we perform a sufficiently large number of trial moves that each involves randomly picking a vertex in the system and slightly perturbing the position of that vertex; we accept all trial moves that decrease  $E$  of the system, which effectively leads to local minimization of  $E$ .

We investigate inherent structures containing the aforementioned three types of topological defects for a wide range of  $p$  (or  $q$ ), as shown in Fig. 2. In the cases of free dislocations and disclinations, we generate structures up to values close to saturation, i.e., more topological defects can no longer be inserted into the system after a sufficiently large number of attempts (e.g.,  $10N$  attempts, where  $N$  is the number of vertices in the lattice). In the case of bound dislocations, we stop at  $p = 0.17$  since increasing  $p$  beyond that sometimes leads to unphysical local bonding networks (e.g., bonds that cross each other).

### III. STRUCTURAL CHARACTERIZATION AND HYPERUNIFORMITY

We generate configurations with  $N = 10\,800$  particles and look at various statistics including pair statistics such as  $g_2(r)$ ,  $S(k)$ , and  $\sigma_N^2(R)$  [1,2], and bond-orientational statistics such as the bond-orientational order metric  $Q_6$  and correlation function  $C_6(r)$  that have been routinely used to study the two-dimensional (2D) melting process [36–38]. To compute the statistics accurately, we average over 10 configurations at each  $p$  (or  $q$ ).

Specifically, the pair correlation function  $g_2(r)$  is proportional to the probability density function of finding two centers separated by distance  $r$  [39], and in practice is computed via the relation

$$g_2(r) = \frac{\langle N(r) \rangle}{\rho 2\pi r \Delta r}, \quad (2)$$

where  $\langle N(r) \rangle$  is the average number of particle centers that fall into the circular ring at distance  $r$  from a central particle center (arbitrarily selected and averaged over all particle centers in the system),  $2\pi r \Delta r$  is the area of the circular ring, and  $\rho$  is the number density of the system [31,39]. The static structure factor  $S(k)$  is the Fourier counterpart and, for computational purposes,  $S(k)$  is the angular-averaged version of  $S(\mathbf{k})$ , which can be obtained directly from the particle positions  $\mathbf{r}_j$ , i.e.,

$$S(\mathbf{k}) = \frac{1}{N} \left| \sum_{j=1}^N \exp(i\mathbf{k} \cdot \mathbf{r}_j) \right|^2 \quad (\mathbf{k} \neq \mathbf{0}), \quad (3)$$

where  $N$  is the total number of points in the system [3,6,31]. The trivial forward scattering contribution ( $\mathbf{k} = \mathbf{0}$ ) in Eq. (3) is omitted, which makes Eq. (3) completely consistent with the aforementioned definition of  $S(k)$  in the ergodic infinite-system limit [2]. To compute  $\sigma_N^2(R)$ , we randomly place circular observation windows with radius  $R$  in the system,

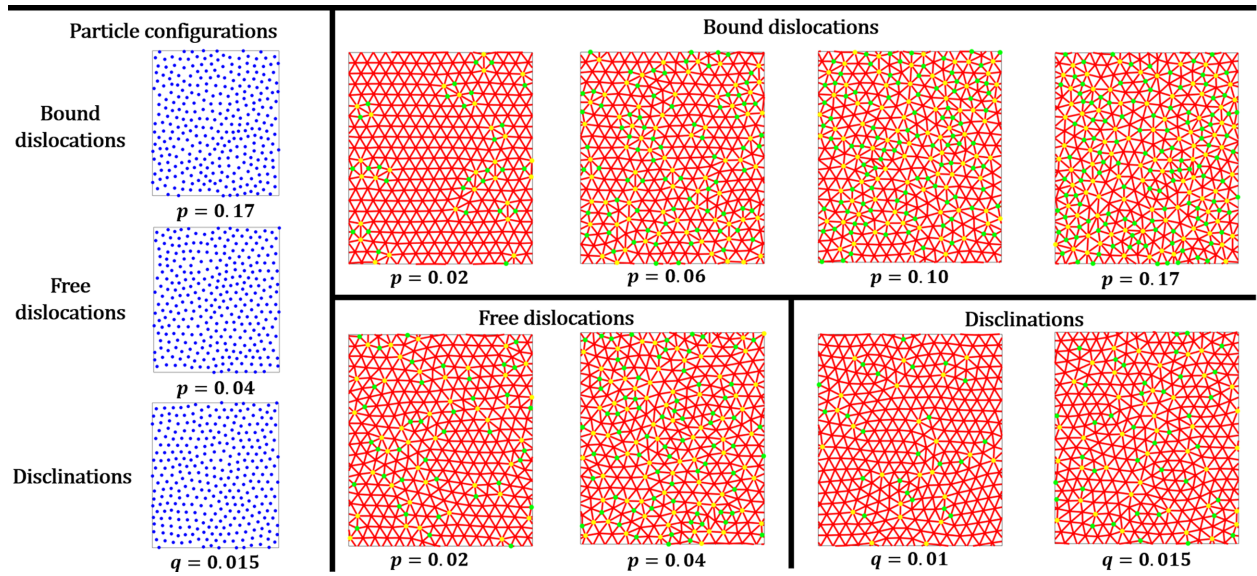


FIG. 2. Left column: Illustration of representative particle configurations associated with inherent structures containing bound dislocations (top), free dislocations (middle), and disclinations (bottom). Right column, top section: Representative inherent structures containing primarily bound dislocations at defect concentration  $p = 0.02, 0.06, 0.10,$  and  $0.17,$  respectively. Right column, bottom-left section: Representative inherent structures containing primarily free dislocations at defect concentration  $p = 0.02$  and  $0.04,$  respectively. Right column, bottom-right section: Representative inherent structures containing disclinations at defect concentration  $q = 0.01$  and  $0.015,$  respectively. Vertices with more than six bonds are highlighted in yellow, and vertices with less than six bonds are highlighted in green.

and count the number of particles,  $N(R)$ , that fall into the observation window, which is a random variable. The variance associated with  $N(R)$  is denoted by  $\sigma_N^2(R) \equiv \langle N(R)^2 \rangle - \langle N(R) \rangle^2$ , which measure density fluctuations of particles within a window of radius  $R$ . In this work, we sample 100 000 windows at each window radius  $R$  to obtain  $\sigma_N^2(R)$ .

On the other hand, the order metric  $Q_6$  is defined as

$$Q_6 \equiv |\langle \Psi_6 \rangle|, \quad (4)$$

where

$$\Psi_6(\mathbf{r}_i) = \frac{1}{n_i} \sum_{j=1}^{n_i} e^{6\theta_{ij}}, \quad (5)$$

$\langle \cdot \rangle$  denotes the ensemble average,  $n_i$  is the number of neighbors of vertex  $i$  located at  $\mathbf{r}_i$ , and  $\theta_{ij}$  is the polar angle associated with the vector from vertex  $i$  to the  $j$ th bonded neighbor of vertex  $i$ . Here we define neighbors as pairs of vertices connected by a bond. The bond-orientational correlation function  $C_6(r)$  is defined as

$$C_6(r) \equiv \langle \Psi_6(\mathbf{r}_i) \Psi_6^*(\mathbf{r}_j) \rangle \mid r = |\mathbf{r}_i - \mathbf{r}_j|, \quad (6)$$

where  $\Psi_6^*$  is the complex conjugate of  $\Psi_6$ . In practice, to calculate  $C_6(r)$ , for each pair of particles located at  $\mathbf{r}_i$  and  $\mathbf{r}_j$ , we compute  $\Psi_6(\mathbf{r}_i) \Psi_6^*(\mathbf{r}_j)$ , and bin the results according to the distance  $r = |\mathbf{r}_i - \mathbf{r}_j|$ . We note that  $Q_6 = 1$  and  $C_6(r) = 1$  for a perfect triangular network, while for an isotropic fluid phase,  $Q_6 \approx 0$  and  $C_6(r)$  decays with an exponential envelope at large  $r$  [36,37].

In Figs. 3 and 4, we present various pair and bond-orientational statistics associated with the inherent structures containing the aforementioned three types of topological

defects, respectively. Interestingly, these inherent structures share many structural similarities, despite the different defect types. In particular, these inherent structures preserve the class-I hyperuniformity of the triangular lattice, as manifested by the fact that  $S(k)$  essentially decreases to zero with an approximately quadratic scaling as  $k$  approaches zero and  $\sigma_N^2(R)$  increases linearly as  $R$  increases at large  $R$ . Both  $h(r)$  and  $C_6(r)$  decay to their respective long-range values over a short length scale, and the long-range value of  $|g_2(r) - 1|$ , the magnitudes of the Bragg peaks in  $S(k)$ , and  $Q_6$  decrease rapidly as  $p$  or  $q$  increases, indicating the loss of large-scale structural order as topological defects are introduced into the system. Here we note that the absence of Bragg peaks alone does not guarantee that the underlying structure is truly amorphous since long-range order can be hidden at the two-body level, but still can be present in higher-order correlations, as explicitly demonstrated by Klatt *et al.* in the context of random, uncorrelated displacements of particles on a lattice [40]. There are also clear wiggles in  $S(k)$  at large  $k$  and significant oscillations in  $g_2(r)$ , which are manifestations of the remaining short-range structures in the defected networks. Moreover, we note that at comparable defect concentrations, disclinations degrade the translational and orientational order of the triangular lattice the most, followed by free dislocations and bound dislocations, as evidenced by  $g_2(r)$ ,  $C_6(r)$ , and  $Q_6$ . It is not surprising that the impact of bound dislocations are much more localized than that of free dislocations and disclinations.

It is noteworthy that in colloidal systems during 2D melting, as free dislocations begin to emerge, the systems start to enter the hexatic phase regime, and the  $h(r)$  and  $C_6(r)$  typically show an exponential and an algebraic decay, respectively [36,37]; on the other hand, the emergence of isolated disclina-

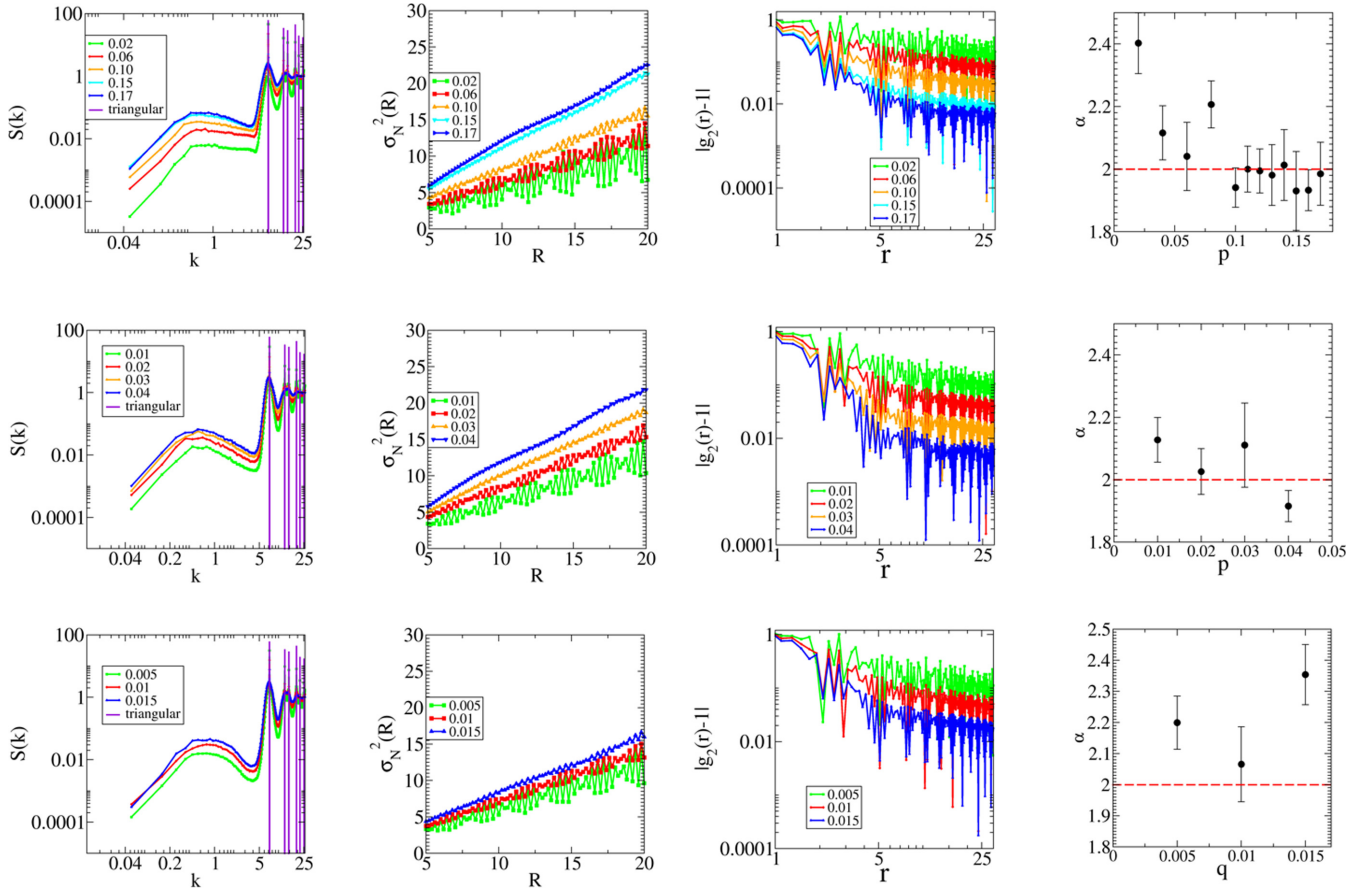


FIG. 3. Pair statistics associated with inherent structures containing primarily bound dislocations (top panel), inherent structures containing primarily free dislocations (middle panel), and inherent structures containing disclinations (bottom panel) at different defect concentrations  $p$  or  $q$  with  $N = 10\,800$  particles. Left to right, Column 1: Log-log plot of structure factor  $S(k)$ . Here we also include the plot for the  $S(k)$  of the corresponding perfect triangular lattice as a reference, which is strictly zero for  $k < K$ , where  $K$  is the location of the first peak. Column 2: Local number variance  $\sigma_N^2(R)$ . Column 3: Log-log plot of  $|g_2(r) - 1|$ . Column 4: Small-wave-number scaling exponent  $\alpha$  of  $S(k)$ , extracted as the slope of linear fittings of  $\ln S(k)$  vs  $\ln k$  for  $k < 0.5$ .

tions typically leads the systems to transition into isotropic liquids, which essentially lose translational and orientational order, i.e.,  $h(r)$  and  $C_6(r)$  both exhibit an exponential decay as  $r$  increases [36,37]. These behaviors are distinctly different from those of our inherent structures containing primarily free dislocations or disclinations, and may be attributed to the fact that in our systems, the free dislocations or disclinations are introduced in a mostly uncorrelated manner, while during 2D melting, the free dislocations or disclinations arise as a result of thermal excitation and possess certain degrees of spatial correlation. Our results suggest that not only the types of topological defects, but also the spatial correlation of topological defects affect the structural behaviors of the defected lattices. Moreover, contrary to our inherent structures, those equilibrium configurations during 2D melting [36,37] are generally not hyperuniform, highlighting the cloaking of hyperuniformity by thermal fluctuations. In fact, our inherent structures will surely lose (perfect) hyperuniformity if thermalized, similar to other hyperuniform structures in general [41]. In addition, we note that the inherent structures containing topological defects such as dislocations and disclinations are distinctively different from other defected lattices such as lattices with random vacancies or lattices with ran-

dom uncorrelated displacements [41,42], since lattices with random vacancies are shown to be nonhyperuniform, while the inherent structures associated with lattices with random uncorrelated displacements are the corresponding perfect lattices and thus ordered.

#### IV. CONTINUUM THEORY OF HYPERUNIFORMITY IN INHERENT STRUCTURES CONTAINING TOPOLOGICAL DEFECTS

In this section, we devise a continuum theory to explain our observations from Sec. III of the impact of the topological defects on hyperuniformity, i.e., how the topological transformations involving dislocations and disclinations preserve the class-I hyperuniformity of the original triangular-lattice crystal. We note that the introduction of topological defects preserves the total number of particles in the system, i.e., no particles were removed or added. Therefore, the impacts on the local number density fluctuations result from the perturbation of particle positions at the core of the defects and the associated elastic displacement field. Specifically, we assume that the particle displacement (at low defect concentrations) at position  $\mathbf{x}$  is the linear superposition of the displacements

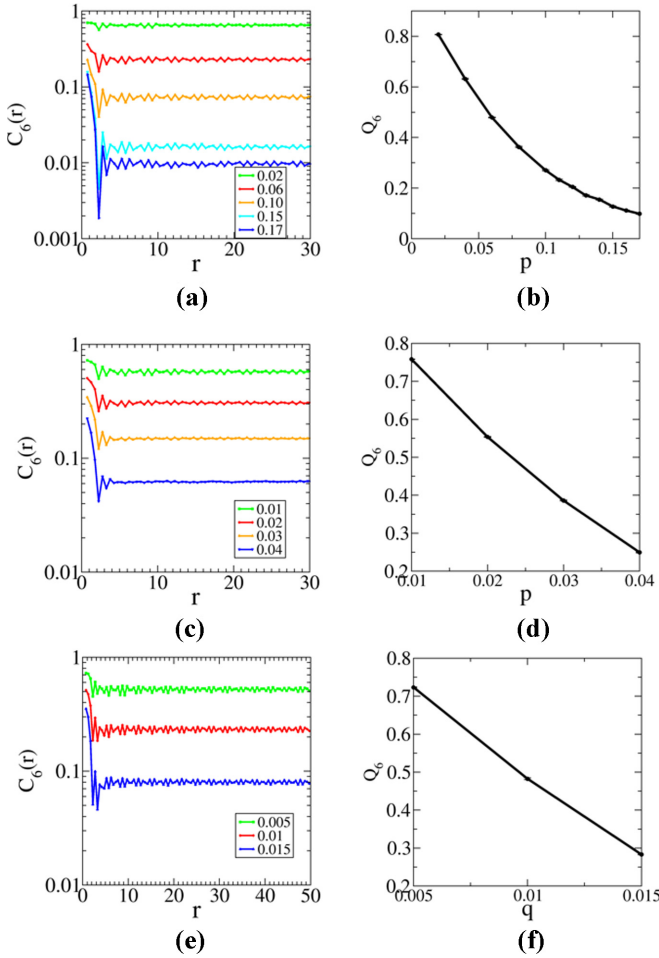


FIG. 4. (a) Bond-orientational order correlation function  $C_6(r)$  and (b) order metric  $Q_6$  of inherent structures containing primarily bond dislocations at different defect concentrations  $p$  with  $N = 10\,800$  particles. (c) Bond-orientational order correlation function  $C_6(r)$  and (d) order metric  $Q_6$  of inherent structures containing primarily free dislocations at different defect concentrations  $p$  with  $N = 10\,800$  particles. (e) Bond-orientational order correlation function  $C_6(r)$  and (f) order metric  $Q_6$  of inherent structures containing disclinations at different defect concentrations  $q$  with  $N = 10\,800$  particles.

introduced by different topological defects (i.e., strain sources) at  $\mathbf{r}_1, \dots, \mathbf{r}_M$ , where  $M$  is the number of topological defects, i.e.,

$$\mathbf{u}(\mathbf{x}) = \sum_{i=1}^M \mathbf{f}(\mathbf{x} - \mathbf{r}_i), \quad (7)$$

and where the  $\mathbf{f}$  functions are the sources. Therefore, the average displacement field  $\langle \mathbf{u}(\mathbf{x}) \rangle$  is given by

$$\begin{aligned} \langle \mathbf{u}(\mathbf{x}) \rangle &= \int \sum_{i=1}^M \mathbf{f}(\mathbf{x} - \mathbf{r}_i) P_M(\mathbf{r}^M) d\mathbf{r}^M \\ &= \int \mathbf{f}(\mathbf{x} - \mathbf{r}_1) \rho_{1s}(\mathbf{r}_1) d\mathbf{r}_1 \\ &= \rho_s \int \mathbf{f}(\mathbf{r}) d\mathbf{r}, \end{aligned} \quad (8)$$

where  $P_M(\mathbf{r}^M)$  is the probability density function [1] associated with finding defects  $1, 2, \dots, M$  at position  $\mathbf{r}_1, \mathbf{r}_2, \dots, \mathbf{r}_M$ , and  $\rho_{ms}(\mathbf{r}^m)$  ( $m < M$ ) is the reduced generic density function [1] of the defects defined as

$$\rho_{ms}(\mathbf{r}^m) = \frac{M!}{(M-m)!} \int \dots \int P_M(\mathbf{r}^M) d\mathbf{r}^{M-m}, \quad (9)$$

and because of statistical homogeneity, the one-point density function  $\rho_{1s}(\mathbf{r}_1)$  is equal to the average defect density  $\rho_s$  in the system. Similarly, the different components of the displacement-displacement correlation  $\Psi_{\mu\nu}(\mathbf{r} = \mathbf{y} - \mathbf{x}) \equiv \langle u_\mu(\mathbf{x}) u_\nu(\mathbf{y}) \rangle - \langle u_\mu(\mathbf{x}) \rangle \langle u_\nu(\mathbf{y}) \rangle$  are given by

$$\begin{aligned} \Psi_{\mu\nu}(\mathbf{r}) &= \int \sum_{i=1}^M \sum_{j \neq i}^M f_\mu(\mathbf{x} - \mathbf{r}_i) f_\nu(\mathbf{y} - \mathbf{r}_j) P_M(\mathbf{r}^M) d\mathbf{r}^M \\ &+ \int \sum_{i=1}^M f_\mu(\mathbf{x} - \mathbf{r}_i) f_\nu(\mathbf{y} - \mathbf{r}_i) P_M(\mathbf{r}^M) d\mathbf{r}^M \\ &- \int \rho_s^2 f_\mu(\mathbf{x} - \mathbf{r}_1) f_\nu(\mathbf{y} - \mathbf{r}_2) d\mathbf{r}_1 d\mathbf{r}_2 \\ &= \int \rho_s^2 h_s(\mathbf{r}_2 - \mathbf{r}_1) f_\mu(\mathbf{x} - \mathbf{r}_1) f_\nu(\mathbf{y} - \mathbf{r}_2) d\mathbf{r}_1 d\mathbf{r}_2 \\ &+ \int \rho_s f_\mu(\mathbf{x} - \mathbf{r}_1) f_\nu(\mathbf{y} - \mathbf{r}_1) d\mathbf{r}_1, \end{aligned} \quad (10)$$

where  $h_s(\mathbf{r}) \equiv g_{2s}(\mathbf{r}) - 1 = [\rho_{2s}(\mathbf{r}) - \rho_s^2] / \rho_s^2$  is the total correlation function of the topological defects. If the topological defects are randomly introduced into the system, then  $h_s(\mathbf{r}) = 0$ , which gives

$$\begin{aligned} \Psi_{\mu\nu}(\mathbf{r}) &= \int \rho_s f_\mu(\mathbf{x} - \mathbf{r}_1) f_\nu(\mathbf{y} - \mathbf{r}_1) d\mathbf{r}_1 \\ &= \int \rho_s f_\mu(\mathbf{r}_1) f_\nu(\mathbf{r}_1 + \mathbf{r}) d\mathbf{r}_1. \end{aligned} \quad (11)$$

In the Fourier space, this corresponds to

$$\tilde{\Psi}_{\mu\nu}(\mathbf{k}) = \rho_s \tilde{f}_\mu(\mathbf{k}) \tilde{f}_\nu^*(\mathbf{k}) = \rho_s \tilde{f}_\mu(\mathbf{k}) \tilde{f}_\nu(-\mathbf{k}), \quad (12)$$

where  $\tilde{\Psi}, \tilde{\mathbf{f}}$  are the Fourier transforms of  $\Psi$  and  $\mathbf{f}$ , respectively, and  $\tilde{\mathbf{f}}^*$  is the complex conjugate of  $\tilde{\mathbf{f}}$ . Here we emphasize that although the topological defects are randomly distributed, the displacements of each lattice site caused by each individual topological defect are correlated, which leads to overall *correlated displacement fields* in our systems. This differentiates our systems from the perturbed lattice models with uncorrelated displacement fields studied in previous works [40,41].

Next, we derive the expression for the structure factor  $S(k)$  of triangular lattice affected by displacement fields  $\mathbf{u}$ . Previously, it was shown [41] in general that when the displacement field has a finite variance  $\langle |\mathbf{u}|^2 \rangle$  and the displacement-displacement correlation matrix is isotropic and diagonalized, i.e.,  $\Psi_{\mu\nu}(\mathbf{r}) = \delta_{\mu\nu} \Psi(\mathbf{r})$ , the structure factor  $S(\mathbf{k})$  of a displaced hyperuniform point pattern at small  $|\mathbf{k}|$  is approximated by

$$\begin{aligned} S(\mathbf{k}) &\approx \{ |\mathbf{k}|^2 \Psi(\mathbf{0}) + [1 - |\mathbf{k}|^2 \Psi(\mathbf{0})] S_0(\mathbf{k}) \} \\ &+ \rho_0 |\mathbf{k}|^2 \left[ \tilde{\Psi}(\mathbf{k}) + \int d(\mathbf{r}) h_0(\mathbf{r}) \Psi(\mathbf{r}) e^{-i\mathbf{k}\cdot\mathbf{r}} \right], \end{aligned} \quad (13)$$

where  $S_0(\mathbf{k})$  and  $h_0(\mathbf{r})$  are the structure factor and total correlation function of the original point patterns. In the cases where the original point patterns are crystals, we can use the properties of crystals to simplify Eq. (13). In particular, the structure factor  $S_0(\mathbf{k}) = 0$  holds for  $|\mathbf{k}| < K$ , where  $K$  is the wave number associated with the first Bragg peaks, and the pair correlation function  $g_{20}(\mathbf{r}) = h_0(\mathbf{r}) + 1$  is simply a collection of  $\delta$  functions at lattice sites and zero otherwise. By Taylor expanding the second line of Eq. (13) at small  $k$  and invoking the continuum approximation, we obtain the following expression:

$$\begin{aligned} S(k) &\approx k^2 \Psi(0) + \rho_0 k^2 \tilde{\Psi}(0) \\ &= \rho_s k^2 \int f_1^2(\mathbf{r}) d\mathbf{r} + \rho_0 \rho_s k^2 |\tilde{f}_1(0)|^2 \\ &= \rho_s k^2 \int f_2^2(\mathbf{r}) d\mathbf{r} + \rho_0 \rho_s k^2 |\tilde{f}_2(0)|^2. \end{aligned} \quad (14)$$

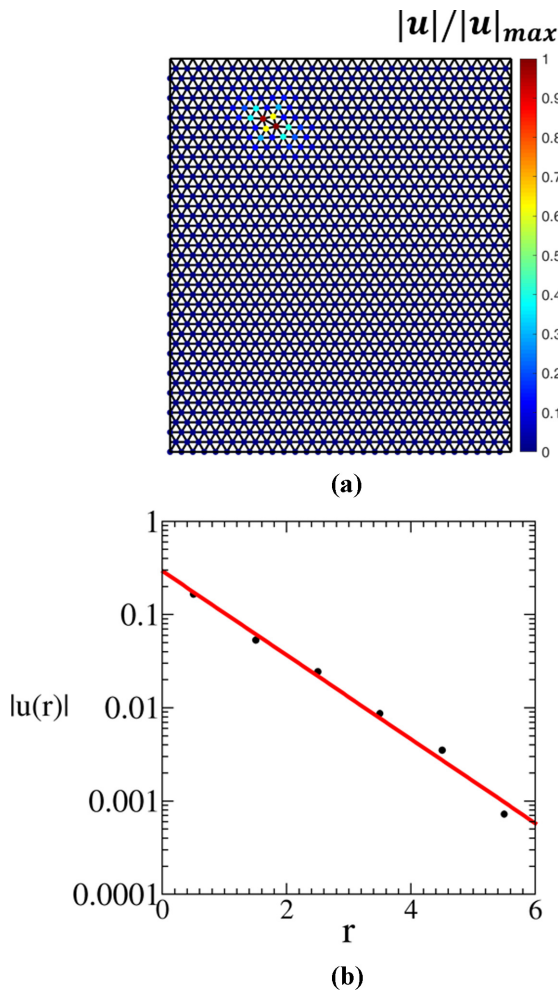


FIG. 5. Displacement field  $\mathbf{u}$  in an inherent structure containing a single pair of bound dislocations. (a) Spatial distribution of normalized  $|u(r)|/|u(r)|_{\max}$ . (b) Decay of  $|u(r)|$  as a function of the distance  $r$  from the core of the topological defect, i.e., the center of the old broken bond (the same as the center of the new formed bond), and the red solid line is an exponential fit (note that the vertical axis is a logarithmic scale).

Interestingly, Eq. (14) suggests that as long as the volume integrals of  $\mathbf{f}(\mathbf{r})$  and  $|\mathbf{f}(\mathbf{r})|^2$  are finite, the structure factor  $S(k)$  of the triangular lattice affected by the displacement fields generated by the collection of randomly distributed source functions  $\mathbf{f}$  scales as  $S(k) \sim k^2$ , which indicates that such displacement fields preserve the class-I hyperuniformity of the original crystals.

We then test our continuum theory against our numerical simulations of representative inherent structures. In Fig. 5(a), we first visualize the magnitude of the displacement field  $\mathbf{u}$  in an inherent structure containing a single pair of bound

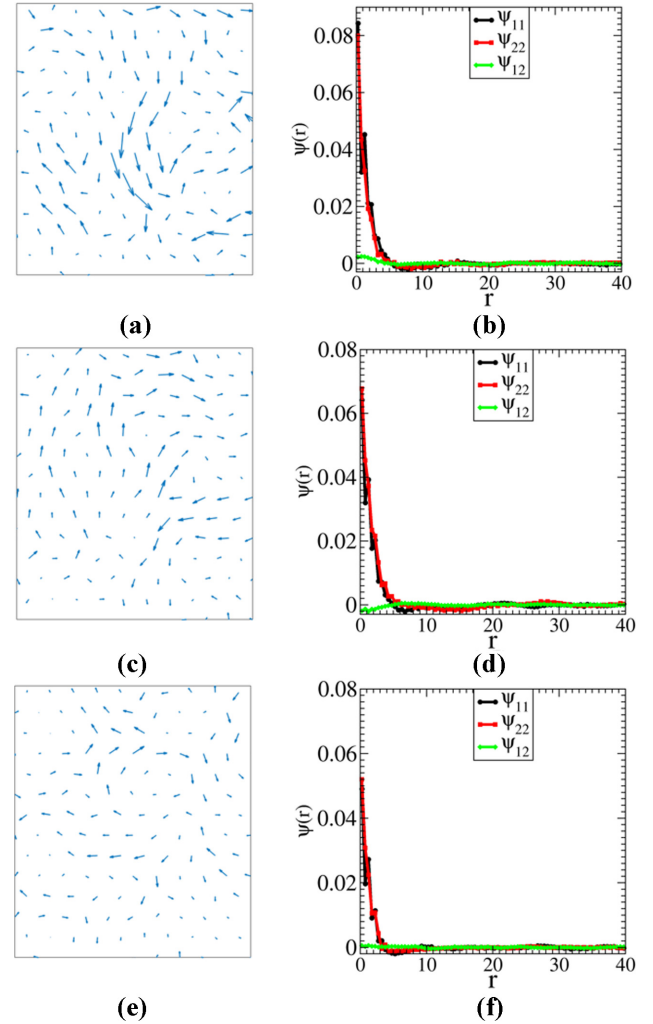


FIG. 6. (a) Visualization of spatial distribution of the vector displacement field  $\mathbf{u}(\mathbf{r})$  and (b) plot of the displacement-displacement correlation matrix  $\Psi(r)$  in an inherent structure containing primarily bound dislocations at  $p = 0.17$ . (c) Visualization of spatial distribution of the vector displacement field  $\mathbf{u}(\mathbf{r})$  and (d) plot of the displacement-displacement correlation matrix  $\Psi(r)$  in an inherent structure containing primarily free dislocations at  $p = 0.04$ . (e) Visualization of spatial distribution of the vector displacement field  $\mathbf{u}(\mathbf{r})$  and (f) plot of the displacement-displacement correlation matrix  $\Psi(r)$  in an inherent structure containing disclinations at  $q = 0.015$ . The visualizations are using representative portions of configurations with  $N = 1200$  particles, while the correlation matrices are computed using configurations with  $N = 10\,800$  particles.

dislocations. Clearly, the displacement field concentrates around the center of the topological defect, i.e., the center of the old broken bond (which is the same as the center of the new formed bond). We further compute the decay of  $|\mathbf{u}(r)|$  as a function of the distance  $r$  from the core of the topological defect, which appears to decay exponentially, as shown in Fig. 5(b), although we note that  $|\mathbf{u}(\mathbf{r})|$  appears to be anisotropic around the core, as shown in Fig. 5(a). The exponential decay clearly suggests that the volume integrals of the source  $\mathbf{f}$  and  $|\mathbf{f}|^2$  should be finite in this case.

We then look at the cases where substantial amounts of topological defects are affecting the structures. Specifically, in Fig. 6, we show the spatial distribution of the vector displacement field  $\mathbf{u}(\mathbf{r})$  and compute the corresponding displacement-displacement correlation matrices  $\Psi(r)$  for three representative examples: an inherent structure containing primarily bound dislocations at  $p = 0.17$ , an inherent structure containing primarily free dislocations at  $p = 0.04$ , and an inherent structure containing disclinations at  $q = 0.015$ . All three fields in the visualizations appear to be approximately isotropic on large scales, suggesting finite  $\tilde{\Psi}(0)$  and thus finite volume integrals of  $\mathbf{f}(\mathbf{r})$ ; on the other hand, we observe that  $\Psi_{12} \approx 0$ ,  $\Psi_{11}(r) \approx \Psi_{22}(r)$ , and  $\Psi_{11}(0)$  or  $\Psi_{22}(0)$  are finite, which indicates that  $\Psi_{\mu\nu}(\mathbf{r}) = \delta_{\mu\nu}\Psi(\mathbf{r})$  and volume integrals of  $|\mathbf{f}(\mathbf{r})|^2$  are finite, satisfying the assumptions in our theory. Next, we proceed to investigate whether the numerically determined small- $k$  behavior of  $S(k)$  of our inherent structures matches the prediction by our theory. The scaling exponent  $\alpha$  in  $S(k) \sim k^\alpha$  at small  $k$  shown in Fig. 3 is extracted as the slope of linear fittings of  $\ln S(k)$  vs  $\ln k$  for  $k < 0.5$ . As mentioned above, the unit length is set as the side length of a triangle in a perfect triangular lattice. Indeed, at low defect concentrations,  $\alpha$  oscillates around 2, matching the quadratic scaling predicted by our theory; however, at very small or large defect concentrations (relative to saturation), the exponent  $\alpha$  slightly deviates from 2. The deviation at very small defect concentrations can be attributed to the fact that at these defect concentrations, the systems are not entirely homogeneous, which degrades the accuracy of our continuum-theory prediction; on the other hand, at large defect concentrations, the topological defects begin to interact with each other and modify the inherent structures accordingly, which is not taken into account in our continuum theory.

## V. CONCLUSIONS AND DISCUSSION

In this work, using representative numerical examples and theoretical analysis, we demonstrate that disordered inherent structures that are topological variants of crystals preserve the class-I hyperuniformity of the crystals as long as the topological defects are randomly introduced, the displacement fields generated by individual topological defects are sufficiently localized (i.e., the volume integrals of the displacements and

squared displacements caused by individual defect are finite), and the displacement-displacement correlation matrix of the system is diagonalized and isotropic on large length scales. These results are universal, regardless of the exact defect types and concentrations. Moreover, the inherent structures containing dislocations and disclinations studied in this work are quite different from the equilibrium structures containing the same type of topological defects in colloidal systems during 2D melting [36,37], suggesting that not only the types of defects, but also the spatial correlations of defects are key to understanding the impact of defects on the structural features of crystalline systems. Our numerical results and theoretical analysis uncover the mechanisms underlying the emergence of disordered hyperuniformity in a wide spectrum of disordered structures, and provide insights to the discovery, design, and generation of novel disordered hyperuniform materials.

It is noteworthy that topological defects such as dislocations and disclinations appear as point defects in two dimensions, while in three dimensions they are known to appear as line defects. Given this difference, it would be interesting to explore the impact of topological defects on the large-scale structural features of crystals in three dimensions, and the potential findings may shed light on the emergence of hyperuniformity in certain disordered inherent structures. For example, there were theories [35] suggesting that MRJ packings (or random close packings as termed by many experimentalists) might be considered as disordered topological variants of the tetrahedral particle packings, just as Frank-Kasper phases [35,43,44] are considered as ordered topological variants.

In addition, we note that here we have investigated the introduction of topological defects into the triangular lattice, but given the duality of the triangular lattice and honeycomb lattice, the duals of the various inherent structures obtained in this work are similar to the network structures obtained previously [45] that are topologically transformed from the honeycomb lattice through the introduction of Stone-Wales (SW) defects, which are relevant to amorphous graphene and other 2D materials [45]. However, previously it was demonstrated that as the SW defect concentration reaches a certain critical value, the corresponding systems change from class-I hyperuniformity to class-II hyperuniformity, which can be attributed to the fact that in those systems, the bond angles were also regulated because of the underlying chemical constraints [45] and the additional coupling between defects likely modifies the behavior of large-scale density fluctuations and leads to the change in the class of hyperuniformity at sufficiently large defect concentrations.

## ACKNOWLEDGMENT

We are grateful for Dr. Jaeuk Kim for the very helpful discussion.

- [1] S. Torquato and F. H. Stillinger, Local density fluctuations, hyperuniformity, and order metrics, *Phys. Rev. E* **68**, 041113 (2003).  
 [2] S. Torquato, Hyperuniform states of matter, *Phys. Rep.* **745**, 1 (2018).

- [3] C. E. Zachary and S. Torquato, Hyperuniformity in point patterns and two-phase random heterogeneous media, *J. Stat. Mech. Theor. Expt.* (2009) P12015.  
 [4] C. E. Zachary, Y. Jiao, and S. Torquato, Hyperuniform Long-Range Correlations are a Signature of Disordered



- Jammed Hard-Particle Packings, *Phys. Rev. Lett.* **106**, 178001 (2011).
- [5] Y. Jiao and S. Torquato, Maximally random jammed packings of platonic solids: Hyperuniform long-range correlations and isostaticity, *Phys. Rev. E* **84**, 041309 (2011).
- [6] D. Chen, Y. Jiao, and S. Torquato, Equilibrium phase behavior and maximally random jammed state of truncated tetrahedra, *J. Phys. Chem. B* **118**, 7981 (2014).
- [7] C. E. Zachary and S. Torquato, Anomalous local coordination, density fluctuations, and void statistics in disordered hyperuniform many-particle ground states, *Phys. Rev. E* **83**, 051133 (2011).
- [8] S. Torquato, G. Zhang, and F. H. Stillinger, Ensemble Theory for Stealthy Hyperuniform Disordered Ground States, *Phys. Rev. X* **5**, 021020 (2015).
- [9] A. Donev, F. H. Stillinger, and S. Torquato, Unexpected Density Fluctuations in Jammed Disordered Sphere Packings, *Phys. Rev. Lett.* **95**, 090604 (2005).
- [10] R. D. Batten, F. H. Stillinger, and S. Torquato, Novel Low-Temperature Behavior in Classical Many-Particle Systems, *Phys. Rev. Lett.* **103**, 050602 (2009).
- [11] R. Kurita and E. R. Weeks, Incompressibility of polydisperse random-close-packed colloidal particles, *Phys. Rev. E* **84**, 030401(R) (2011).
- [12] G. L. Hunter and E. R. Weeks, The physics of the colloidal glass transition, *Rep. Prog. Phys.* **75**, 066501 (2012).
- [13] R. Dreyfus, Y. Xu, T. Still, L. A. Hough, A. G. Yodh, and S. Torquato, Diagnosing hyperuniformity in two-dimensional, disordered, jammed packings of soft spheres, *Phys. Rev. E* **91**, 012302 (2015).
- [14] D. Hexner and D. Levine, Hyperuniformity of Critical Absorbing States, *Phys. Rev. Lett.* **114**, 110602 (2015).
- [15] R. L. Jack, I. R. Thompson, and P. Sollich, Hyperuniformity and Phase Separation in Biased Ensembles of Trajectories for Diffusive Systems, *Phys. Rev. Lett.* **114**, 060601 (2015).
- [16] J. H. Weijjs, R. Jeanneret, R. Dreyfus, and D. Bartolo, Emergent Hyperuniformity in Periodically Driven Emulsions, *Phys. Rev. Lett.* **115**, 108301 (2015).
- [17] M. Florescu, S. Torquato, and P. J. Steinhardt, Designer disordered materials with large, complete photonic band gaps, *Proc. Natl. Acad. Sci. USA* **106**, 20658 (2009).
- [18] W. Man, M. Florescu, E. P. Williamson, Y. He, S. R. Hashemizad, B. Y. C. Leung, D. R. Liner, S. Torquato, P. M. Chaikin, and P. J. Steinhardt, Isotropic band gaps and freeform waveguides observed in hyperuniform disordered photonic solids, *Proc. Natl. Acad. Sci. USA* **110**, 15886 (2013).
- [19] Y. Jiao, T. Lau, H. Hatzikirou, M. Meyer-Hermann, J. C. Corbo, and S. Torquato, Avian photoreceptor patterns represent a disordered hyperuniform solution to a multiscale packing problem, *Phys. Rev. E* **89**, 022721 (2014).
- [20] A. Mayer, V. Balasubramanian, T. Mora, and A. M. Walczak, How a well-adapted immune system is organized, *Proc. Natl. Acad. Sci. USA* **112**, 5950 (2015).
- [21] M. Hejna, P. J. Steinhardt, and S. Torquato, Nearly hyperuniform network models of amorphous silicon, *Phys. Rev. B* **87**, 245204 (2013).
- [22] M. A. Klatt, J. Lovrić, D. Chen, S. C. Kapfer, F. M. Schaller, P. W. A. Schönhofer, B. S. Gardiner, A. Smith, G. E. Schröder-Turk, and S. Torquato, Universal hidden order in amorphous cellular geometries, *Nat. Commun.* **10**, 1 (2019).
- [23] Q.-L. Lei, M. P. Ciamarra, and R. Ni, Nonequilibrium strongly hyperuniform fluids of circle active particles with large local density fluctuations, *Sci. Adv.* **5**, eaau7423 (2019).
- [24] Q.-L. Lei and R. Ni, Hydrodynamics of random-organizing hyperuniform fluids, *Proc. Natl. Acad. Sci. USA* **116**, 22983 (2019).
- [25] D. Chen and S. Torquato, Designing disordered hyperuniform two-phase materials with novel physical properties, *Acta Mater.* **142**, 152 (2018).
- [26] A. Chremos and J. F. Douglas, Hidden Hyperuniformity in Soft Polymeric Materials, *Phys. Rev. Lett.* **121**, 258002 (2018).
- [27] G. Rumi, J. Aragon Sánchez, F. Elías, R. Cortes Maldonado, J. Puig, N. R. Cejas Bolecek, G. Nieva, M. Konczykowski, Y. Fasano, and A. B. Kolton, Hyperuniform vortex patterns at the surface of type-II superconductors, *Phys. Rev. Research* **1**, 033057 (2019).
- [28] M. Huang, W. Hu, S. Yang, Q.-X. Liu, and H. P. Zhang, Circular swimming motility and disordered hyperuniform state in an algae system, *Proc. Natl. Acad. Sci. USA* **118**, e2100493118 (2021).
- [29] S. Torquato, Swimming in circles can lead to exotic hyperuniform states of active living matter, *Proc. Natl. Acad. Sci. USA* **118**, e2107276118 (2021).
- [30] Y. Jiao, Hyperuniformity of expected equilibrium density distributions of Brownian particles via designer external potentials, *Physica A* **585**, 126435 (2022).
- [31] S. Atkinson, F. H. Stillinger, and S. Torquato, Detailed characterization of rattlers in exactly isostatic, strictly jammed sphere packings, *Phys. Rev. E* **88**, 062208 (2013).
- [32] R. D. Batten, F. H. Stillinger, and S. Torquato, Inherent structures for soft long-range interactions in two-dimensional many-particle systems, *J. Chem. Phys.* **135**, 054104 (2011).
- [33] T. A. Weber and F. H. Stillinger, Local order and structural transitions in amorphous metal-metalloid alloys, *Phys. Rev. B* **31**, 1954 (1985).
- [34] B. I. Halperin and D. R. Nelson, Theory of Two-Dimensional Melting, *Phys. Rev. Lett.* **41**, 121 (1978).
- [35] D. R. Nelson, Order, frustration, and defects in liquids and glasses, *Phys. Rev. B* **28**, 5515 (1983).
- [36] K. Zahn, R. Lenke, and G. Maret, Two-Stage Melting of Paramagnetic Colloidal Crystals in Two Dimensions, *Phys. Rev. Lett.* **82**, 2721 (1999).
- [37] K. Wierschem and E. Manousakis, Simulation of melting of two-dimensional Lennard-Jones solids, *Phys. Rev. B* **83**, 214108 (2011).
- [38] Y.-W. Li and M. P. Ciamarra, Role of cell deformability in the two-dimensional melting of biological tissues, *Phys. Rev. Materials* **2**, 045602 (2018).
- [39] S. Torquato, *Random Heterogeneous Materials: Microstructure and Macroscopic Properties* (Springer-Verlag, New York, 2002).
- [40] M. A. Klatt, J. Kim, and S. Torquato, Cloaking the underlying long-range order of randomly perturbed lattices, *Phys. Rev. E* **101**, 032118 (2020).
- [41] J. Kim and S. Torquato, Effect of imperfections on the hyperuniformity of many-body systems, *Phys. Rev. B* **97**, 054105 (2018).
- [42] A. T. Chicco, R. Dreyfus, and D. J. Durian, Characterizing pixel and point patterns with a hyperuniformity disorder length, *Phys. Rev. E* **96**, 032909 (2017).

- [43] A. Reddy, M. B. Buckley, A. Arora, F. S. Bates, K. D. Dorfman, and G. M. Grason, Stable Frank-Kasper phases of self-assembled, soft matter spheres, *Proc. Natl. Acad. Sci. USA* **115**, 10233 (2018).
- [44] S. M. Barbon, J.-A. Song, D. Chen, C. Zhang, J. Lequieu, K. T. Delaney, A. Anastasaki, M. Rolland, G. H. Fredrickson, M. W. Bates *et al.*, Architecture effects in complex spherical assemblies of (ab)  $n$ -type block copolymers, *ACS Macro Lett.* **9**, 1745 (2020).
- [45] D. Chen, Y. Zheng, L. Liu, G. Zhang, M. Chen, Y. Jiao, and H. Zhuang, Stone-Wales defects preserve hyperuniformity in amorphous two-dimensional networks, *Proc. Natl. Acad. Sci. USA* **118**, e2016862118 (2021).